

This is the accepted manuscript of the following article:

Ulises Rojas-Alva, Frederik Møller-Poulsen, Sze-Lok Man, Cameron Creamer, David Hanna, Grunde Jomaas

Flame spread behaviour of Polydimethylsiloxane (PDMS) membranes in 1 g and μ g environments

Combustion and Flame

Volume 240

2022

112009,

ISSN 0010-2180

The article has been published in final form at:

<https://doi.org/10.1016/j.combustflame.2022.112009>

And is licensed under:

[CC BY-NC-ND 4.0](https://creativecommons.org/licenses/by-nc-nd/4.0/)

Flame spread behaviour of Polydimethylsiloxane (PDMS) membranes in 1 g and μ g environments

Ulises Rojas-Alva¹, Frederik Møller-Poulsen¹, Sze-Lok Man¹, Cameron Creamer¹, David Hanna¹, Grunde Jomaas^{1,2}

¹School of Engineering, University of Edinburgh, Colin MacLaurin Road,

² FRISSBE, ZAG – Slovenian National Building and Civil Engineering Institute, Dimičeva 12,
1000 Ljubljana, Slovenia

Abstract

Diffusion flame behaviour and silica ash (SiO_2) production were experimentally studied for various Polydimethylsiloxane (PDMS) membrane thicknesses (0.125 mm to 1.0 mm) in normal gravity and during microgravity flight experiments. The flames were established on vertical samples (300 mm in length) and subjected to either opposed or concurrent forced flows (both laminar and turbulent), assimilating the NASA Test 1 that is in use for spacecraft material selection. The opposed flame spread rate was observed to be steady and could be estimated using classical theory. Under concurrent flow, the flame spread rate was only steady for very high forced flows. The opposed flame-spread rate ranged from 0.5 to 1.5 mm/s, while the concurrent case ranged between 0.1 and 12 mm/s. The transport of silica ash (SiO_2) was found to affect the heat balance of the concurrent flame spread in a manner that resulted in unsteady flame spread. For opposed flame spread, on the other hand, the transport of silica ash showed to be irrelevant. The extinction behaviour for the concurrent flame spread was heavily dominated by the transport of silica-ash, while for opposed flames, extinction was due to kinetics (at high forced flows). In microgravity environments, the transport and deposition of silica ash is anticipated to dominate flame spread and near-limit as well. These results suggest that silica-based products might be less flammable in microgravity than other similar materials such as common thermoplastics (PP or PE) used as wire jackets.

Keywords: silicone burning, spacecraft fire safety, flame spread, near-limit, silica-ash

Nomenclature

A_g	Gas-phase pre-exponential factor ($\text{m}^3/\text{kg s}$)	T_f	Flame temperature (K)
α_g	Mass diffusivity (m^2/s)	T_g	Gas temperature (K)
α_m	Thermophoretic parameter	T_o	Ambient temperature (K)
c_1	Constant (See Equation 3)	T_p	Pyrolysis temperature (K)
c_2	Constant (See Equation 3)	t_{chem}	Chemical time (s)
c_s	Specific heat of the PDMS membrane ($\text{J}/\text{kg} \cdot \text{K}$)	τ_{flow}	Flow time (s)
c_{SiO_2}	Specific heat of silica-ash ($\text{J}/\text{kg} \cdot \text{K}$)	τ	Half-thickness of PDMS membrane (mm)
Da	Damköhler number (-)	τ_{SiO_2}	Half-thickness of PDMS membrane (mm)
ρ_g	Gas density (kg/m^3)	V_g	Forced flow velocity (mm/s)
ρ_s	Density of PDMS membrane (kg/m^3)	$V_{f,c}$	Concurrent flame spread rate (mm/s)
ρ_{SiO_2}	Density of silica-ash (kg/m^3)	$V_{f,o}$	Opposed flame spread rate (mm/s)

E_g	Gas-phase activation energy (J/mol)	V_{nb}	Buoyancy-driven flow (mm/s)
Φ	Ratio of Solid-heat conduction to the heat conduction through the gas-phase	U_t	Thermophoretic velocity (mm/s)
g	Gravity (m/s ²)	ν	Dynamic viscosity (kg/m s)
l_h	Characteristic pre-heat length (m)	$Y_{o,\infty}$	Mass fraction of oxidiser (-)
λ_g	Gas-phase thermal conductivity (W/m K)	Y_{Fs}	Mass fraction of species (-)
λ_s	Solid-phase thermal conductivity (W/m K)	ΔH_R	Heat of combustion(kJ/kg)
R	Universal gas constant (J/mol · K)	x_{ext}	Distance to the point of extinguishment (mm)

1. INTRODUCTION

Due to their range of useful properties, such as inherent fire retardancy, silicone-based products have a wide application, including use in spacecraft [1]. The term silicone covers a large group of polymers containing silicon atoms. The material is often simply referred to as silicone, which results in a range of material parameters [1]. Silicones have high thermal stability, are non-corrosive, are gas permeable and electrically resistant [2]. Therefore, not all silicones have the same properties. In addition, silicone-based materials are known to be less flammable than other materials with similar use.

During thermal decomposition of silicone in oxidative environments, the combustion products react to form amorphous silica ash (SiO₂), water, carbon dioxide and other compounds. The amorphous silica ash (SiO₂) is a by-product that forms during thermal degradation and during the gas-phase near the combustion field. During flaming, the silica-ash production is significant [3]. The silica-ash deposits on the unburnt fuel form a protective layer that inhibits further decomposition [4]. Such a layer acts as an insulation barrier; thus, the fuel is protected from any heat (especially from the flame), and the fuel does not reach the pyrolysis temperature. This is a behaviour that has similarities with those reported for charring materials such as wood. However, silica ash differs from charring materials as the ash forms in the gas-phase, whereas char forms in the solid phase. Additionally, during thermal degradation, silicones or siloxanes can form silica in the solid-phase as well [5].

Due to the abovementioned properties, especially the fire retardancy, silicone-based materials or materials with silicone coatings have a particular interest in spacecraft applications. On spacecraft, silicones are used for wire insulation, as filters, for life-support systems, and as coatings for other materials. To assess the fire retardancy, or more appropriately the flammability, of any material for spacecraft applications, these undergo the NASA-STD-6001B Test 1 and Test 2 [6]. In Test 1, the material is subjected to an upwards flame spread based on a buoyant scenario. The criterion to pass or fail the test is defined by the burnt length (15 cm). A particular silicone sheet, the polydimethylsiloxane (PDMS) membrane, used for spacecraft life support systems, passes the criterion successfully for specific thicknesses [7]. However, such a test has been subjected to criticism since it does not represent microgravity scenarios. Hence, a direct extrapolation from Test 1 to microgravity should be done cautiously.

Testing in microgravity environments is both challenging and costly and has in the past primarily been completed in drop towers and parabolic flights [8]. These platforms limit the size of the sample significantly and the time frame over which testing can be conducted. Recently, NASA's Spacecraft Fire Experiments (Saffire) test series was designed to address the knowledge gaps identified in two recent papers [9,10]. Specifically, these tests focused on testing materials over long periods and with larger dimensions than had previously been possible in microgravity experiments. PDMS membranes were tested along with other materials in microgravity during Saffire II, where four samples were subjected to opposed and concurrent forced flows. The goal was to study the corresponding opposed flame (travels against the flow) and concurrent flame (travels along with the flow). Contrary to expectation based on ground experiments, the PDMS samples did not develop self-sustained flames, but were rather extinguished in all cases. These results highlight the need for additional fundamental information about PDMS and silicone-based materials' flammability for spacecraft applications.

Although the silica ash production and deposition on the unburnt fuel provide a positive outcome (fire retardancy), it is incredibly challenging for established models to predict the opposed and concurrent flame spread when silica ash is produced. As mentioned, there is a vast range of silicone materials whose properties depend on the molecular weight and additives for each silicone-based product [11]. Consequently, the exact composition of any specific product and its fundamental combustion properties remains unknown; one clear example is the PDMS membrane sheets. Furthermore, the silica ash deposition can affect any attempt to measure combustion properties, such as heat of combustion, activation energies and pre-exponential factors in oxidative environments [3]. In literature, one can find many articles on the thermal decomposition of silicone in non-oxidative environments [5,12–18], but a few focus on the burning and flammability behaviour of silicones [3,19–22]. It is expected as thermal degradation studies are important for manufacturing silicone products.

The transport and deposition of amorphous silica ash can be affected by the direction of the forced flow interacting with the flame spread. Flame spread under opposed or concurrent forced flows are fundamentally the same, independently of the material type or environmental conditions. In other words, the mechanisms driving the flame remain the same in both scenarios, and these mechanisms are the heat transfer (due to conduction, convection and radiation), diffusion of gases and the chemistry in the gas-phase. However, for practical reasons, many authors provide a different theoretical approach for each of the two scenarios (opposed or concurrent) [23]. Although the three modes of heat transfer (convection, radiation and conduction) all play a role in both scenarios, the importance of each heat transfer mode can differ with environmental conditions, the flame geometry and the flow directions [24].

The contrast between both flame spread cases is the magnitude of the characteristic lengths and the dominant heat transfer. For flame spread under opposed forced flows, the heat transfer at the leading edge (due to heat from the gas-phase to the solid-phase, radiation from the flame and surface re-radiation), is the dominant mechanism, and this heat exchange can be quantified in the pre-heat zone (length), see Figure 1 (A). On the contrary, for flame spread under concurrent forced flows, the heat transfer occurs along the entire length of the flame. The characteristic lengths are thus much shorter for the opposed flame than for the concurrent flame, as shown in Figure 1 (B). Thus, one can intuitively expect that opposed flame spread rates are much slower than concurrent flame spread rates, as more energy is transferred back to the solid surface in the latter case.

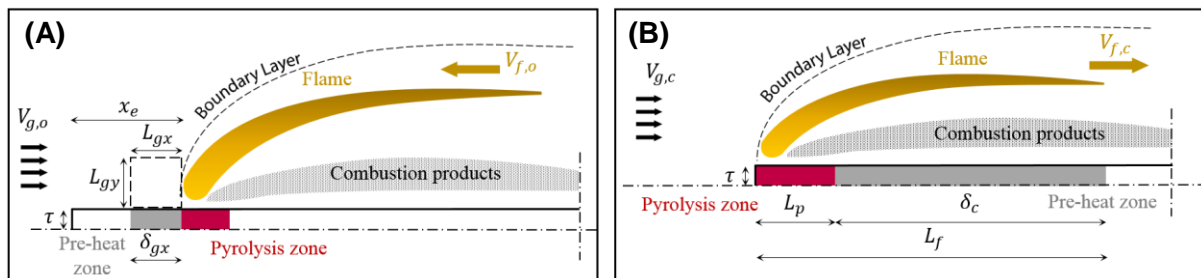


Figure 1 – Schematic of a flame spread in opposed (A) and concurrent (B) forced flows with the characteristic lengths for each case based on the scaling approach from previous studies [25–28].

For the PDMS silicone in this study, where silica (SiO_2) ash is produced during the combustion process, the ash and its deposition on the unburnt fuel can alter the heat transfer mechanisms in both flame cases. Under concurrent forced flows, silica ash has been noted to have a more significant effect [7]. However, under opposed forced flow, the impact of the silica ash remains unclear [7]. During the Saffire II tests, the flame spread could not be self-sustained without the aid of the heating coils [29]. It is interesting to elucidate the leading mechanisms behind the flammability behaviour of PDMS in microgravity. Thereby, the goal of the current study is to understand the effect of flow dynamics on the flammability behaviour (flame spread) of PDMS membranes in normal-gravity and microgravity environments. Particularly, the transport and deposition of silica-ash are of great importance. To achieve this goal, PDMS samples of various thicknesses were tested in a tunnel flow in normal gravity where forced flows were imposed on concurrent and opposed flames. In addition, the microgravity results from Saffire II tests are also analysed and are used to make comparisons with the normal gravity results.

2. EXPERIMENTAL METHOD

The microgravity results were obtained in the Saffire II experiments. The sample cardholder occupied the entire width of the chamber. The distance from the top edge of the sample cardholder to the samples igniter (where the flame starts) was 720 mm, so it is expected that a boundary layer was formed as the incoming forced flow of 20 cm/s encountered the sample card. With the kinematic viscosity of air at 20 °C being $1.516 \times 10^{-5} \text{ m}^2/\text{s}$, the laminar boundary layer thickness is then 37 mm. Thus, the forced flow over the PDMS samples (at the ignition location) was slightly lower than 20 cm/s. Further description of the Saffire II experiments can be found in Jomaas et al. [9].

The normal-gravity experiments were conducted in a purpose-designed rig to study the flame spread behaviour under varied flow configurations. Also, these experiments could be compared to the Saffire II tests as the forced flow and gravity level are the only parameters changing between the microgravity and normal-gravity experiments. The tunnel flow rig consists of three sections, and the lower- and middle-parts act as a flow straightener where the flow is mixed and passed through a honeycomb mesh and as the transition area to the test section, see *Figure 2*. The holder can accommodate samples of 300 mm x 50 mm (same dimensions as used in Saffire II and NASA STD-6001 Test 1). The velocity flow was measured with a hot wire Anemometer (CTV 210-R) at the bottom, middle, and top of the sample's position inside the flow tunnel, and the results of these measurements are shown in *Figure 3*. These flow measurements show that the flow was laminar up to 60-70 cm/s, and a Reynolds number equivalent to 4000 further proves such a limit. After that, the force flow started to become turbulent. Laminar and turbulent flows were considered to be used for the experimental matrix as it was not clear where the extinction limit for flame spread would occur. The flame spread behaviour could then also be evaluated through extinction limits (where the flame no longer propagates).

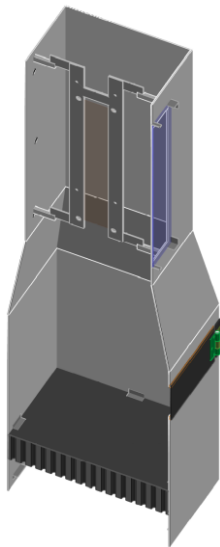


Figure 2 – Schematic of the tunnel flow rig used for the experimental work. The total height of the tunnel is 1 metre. The inner size of the top part and of the bottom part are 0.25 m x 0.25 m and 0.35 m x 0.36 m, respectively.

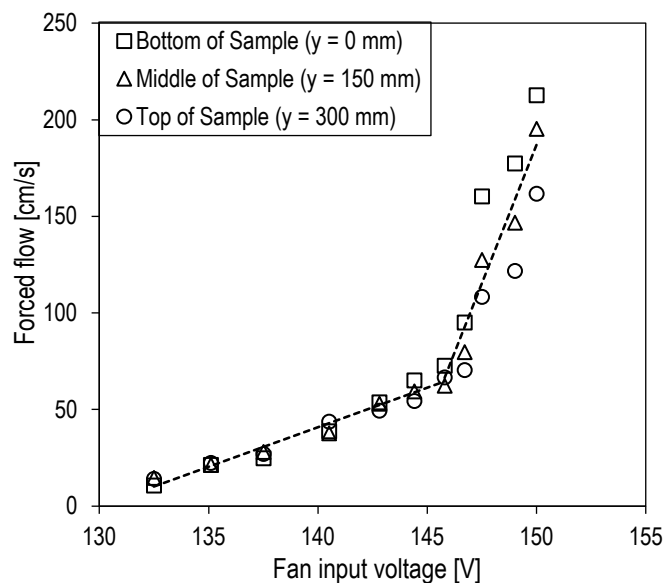


Figure 3 – Flow velocity measurement inside the flow tunnel rig. The location of the measurements is provided in the legend. The values for each data point are an average of three measurements.

A sample PDMS was placed vertically inside the sample holder. Two different ignition mechanisms were used for the laminar flow or turbulent flows. A 23-gauge AWG Nickel-Chromium resistant wire was used for laminar flows, and the wire was energised for up to 10 seconds at 10 A. Thus, the energy provided for ignition was 754 J. The wires were coiled (8 mm diameter) and threaded through seven holes closely spaced across the sample width. For turbulent flows, or where the coils did not achieve ignition, a premixed flame torch was used to attain ignition. The ignition method was applied to the top part of the sample to allow flames to travel downstream (opposed flame spread). When the ignition is applied to the bottom; then, the flame travels upwards (concurrent). The

sample thicknesses were 0.125 mm, 0.152 mm, 0.20 mm, 0.25 mm, 0.36 mm and 0.61 mm. A thermally-thin 0.125 mm PMMA (Acryplen HBS006) sample was also tested, and it was used as reference material to validate the experimental method.

The experiments were recorded with a Canon Camera. The videos were subsequently analysed by a Matlab binary code where the flame leading edge was tracked as a function of time. Thus, the flame spread rate could be estimated. Since two modes of flame spread were studied, a clear distinction has to be made on how the flame spread is defined for each case. For opposed flame spread, the flame length and flame are constant. Thus, the flame spread rate can be taken as the slope of the curve (leading edge position as a function of time). In the concurrent flame spread, the flame length is not necessarily constant, and the flame spread might not be steady during all the process. Therefore, the flame leading edge was monitored, and the flame spread rate was taken when the leading edge showed steadiness.

A minimum of three repetitions was carried out for each set of test conditions. The flame spread rate varied little between repetitions, whereas the burn lengths varied significantly. The standardised pass/fail criteria of 15 cm flame propagation in NASA STD-6001 was used to define whether flame spread belongs to extinction or not. It was expected that the silica ash deposition would affect the concurrent flame spread more than it affected the opposed flame spread.

In the tests where the sample did not fully burn or extinction occurred, small samples of the unburnt fuel were taken to be analysed in a Scanning Electron Microscope (SEM) JEOL JSM-6010 PLUS/LN. The SEM is capable of magnifying to 10 μm – 500 μm and can be used to quantify the deposited silica-ash. For the concurrent experiments, the samples were taken at the point of extinguishment and at various distances (x_{ext}) of 20 mm to 80 mm downwards from that point. For the opposed experiments, samples were taken from the extinguishment edge. Then, the cross-sections of the samples were placed inside the SEM chamber. The images provided by SEM when then processed in 'InfraView' in order to quantify the silica ash thickness.

2.1. Validation of methodology

The flow rig had to be validated, and it was particularly important to ascertain the control of the forced flow parameters in the experimental apparatus. Opposed flame spread is studied since it allows attaining steady conditions, contrarily to the concurrent case. Thus, the flame spread was first studied under the thermal regime where flames were established over the PMMA sample under opposed forced flow (ambient air at atmospheric pressure). Also, using identical solid fuels, the blow-off limits for opposed flame spread were studied following an established theoretical approach. Comparisons were established with literature where the same fuel was used.

To begin, it was examined whether both rigs provided the even forced flow required to attain the thermal regime. The thermal regime for opposed flame spread is characterised by the flame spread rate independence from the oncoming forced flow. This is true for a range of forced flows where the conduction of heat from the gas-phase to the solid-phase at the leading edge dominates the spread phenomenon [23]. Based on the thin-sheet problem, de Ris [30] derived an expression for the opposed flame spread on thermally-thin fuels

$$V_{f,o} = \sqrt{2} \frac{\lambda}{\rho_s c_p \tau} \left(\frac{T_f - T_p}{T_p - T_0} \right) \quad \text{Equation 1}$$

Notice that the equation only portrays heat conduction from the gas-phase to bring the solid-phase to its vaporisation temperature. This formula does not hold when kinetics start to get noticeable (i.e. for increasing forced flows or reduced oxygen concentration). Using de Ris' theoretical expression with the properties of the fuel found in the literature, the flame spread rates were estimated in air under atmospheric conditions. The results of this are presented in *Figure 4*. In the same illustration, the flame spread result conducted in the rig and the data point from other investigations [23] are also plotted. As expected, the current data from both rigs aligns with the theoretical predictions for flows up to 60 cm/s. For flows higher than 60 cm/s, the flame spread rates decrease with increasing forced flow. This behaviour is characterised by kinetics, and Equation 1 cannot be applied.

The data from Takahashi et al. [31–33], only one point coincides with the current data. In the experimental work conducted by Takahashi et al. [31–33], the sample width tested was either 10 mm or 20 mm. As a consequence, their flame spread was three-dimensional in nature and was affected either by side oxygen supply or cooling (three-dimensional effect) [34]. In contrast, the sample used herein was 50 mm in width, and it was not affected by those three-dimensional effects as the flame front only bent closer to the sample's edges. These results confirm that the forced flow provided by the tunnel rig met the initial goal and yielded relevant results.

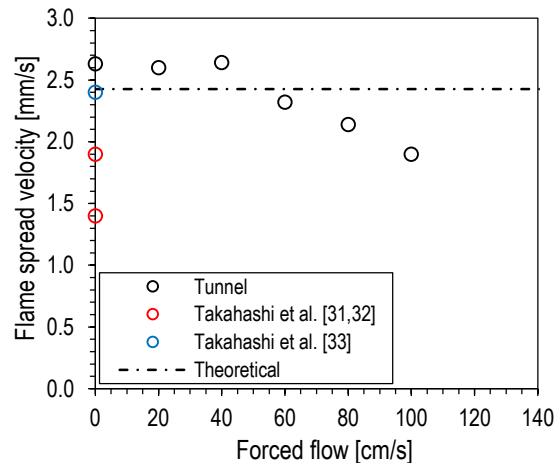


Figure 4 – Theoretical and experimental flame spread velocities for the 0.125 mm thick PMMA sample as a function of the opposed forced flow velocities. The data is from the current study and from Takahashi et al. (2009) [31], Takahashi et al. (2012) [32], and Takahashi et al. (2007) [33].

3. RESULTS AND DISCUSSION

In the following, the experimental results are presented in three sections. In the first sub-chapter, the results from the Saffire II tests are explored and discussed. In the second sub-chapter, the flame spread results in normal gravity are discussed, taking into account the direction of the flow (opposed and concurrent). Additionally, the silica ash residues are discussed quantitatively and qualitatively in the previous sections. Finally, the normal gravity and microgravity flammability limits are compared.

3.1. Flame spread in microgravity (Saffire II)

Images taken during the Saffire II tests for all PDMS samples can be seen in *Table 1*. From the pictures, it is clear that all the samples achieved ignition as flaming combustion occurred. Nonetheless, the flame could not be self-sustained once the ignition wires were turned off. These results were not anticipated [7]. From the extinction images shown in *Table 1*, two main observations can be made. First, the area around the ignition coil is much brighter than the rest of the unburnt sample. These areas clearly indicate an accumulation of silica-ash that has a white colour and thus reflects more light. It is not clear if the ash produced was due to thermal degradation (pyrolysis) or flaming combustion. Second, the videos revealed a white-smoke plume travelling along the forced flow direction; see extinction images for the 0.61 mm and 1.02 mm thick samples in *Table 1*. This white smoke is presumably agglomerated silica-ash (SiO_2) that is transported by the convective forces. Finally, in extinction images, the trail of likely silica-ash is more extensive in the concurrent experiments than in the opposed experiment. Such an observation indicates that the direction of the forced flow might affect the transport of silica-ash in microgravity.

Table 1 – Frames are taken from video recordings of PDMS tests during Saffire II. Each sample had dimensions of 50 mm x 300 mm. The frames are taken during three key events: energising of the ignitor, ignition of sample and diffusion flames, and extinction. In all experiments, the forced flow direction is from right to left, and the flame spread is concurrent and opposed to the forced flow in the corresponding experiments.

Flow direction	Sample thickness	Event	Video frame
Concurrent	0.25 mm	Coil energising (at 2 s)	
		Ignition and flames (at 11 s)	
		Extinction (at 43 s)	
		Post burnt (at 52 s)	
	0.61 mm	Coil energising (at 0 s)	
		Ignition and flames (at 0.26 s)	
		Extinction (at 0.48 s)	
		Post-burnt (at 78 s)	
	1.02 mm	Coil energising (at 3 s)	
		Ignition and flames (at 40 s)	
		Extinction (at 68 s)	
		Extinction (at 82 s)	
Opposed	0.36 mm	Coil energising (at 12 s)	
		Ignition and flames (at 46 s)	
		Extinction (at 66 s)	

Post-burnt
(at 84 s)



The corresponding burnt lengths obtained during the Saffire II test, listed in *Table 2*, are minimal and comply with the NASA Test 1 pass criterion. These results cannot be used to make a certain claim that silicone-based samples are not flammable in microgravity environments. In fact, other polymeric thermally-thin materials have been shown to be more flammable in microgravity conditions [35]. Despite the unexpected outcome of the Saffire II experiments with PDMS, lessons can still be learnt from the little information obtained from the videos. These videos offer interesting information on the flammability behaviour that could be explained with complementary experiments in other microgravity ground-based platforms or normal-gravity data. Hence, the current investigation was motivated to elucidate the flammability behaviour of PDMS in microgravity conditions through a series of normal-gravity experiments.

Table 2 – Burn length results from a preliminary study [7] and from Saffire II [29].

Spread direction	PDMS membrane thickness [mm]	Burn length [mm]	
		1 g [7]	Saffire II, ag [29]
Upwards/concurrent	0.25	27.5	0.0
	0.61	7.6	0.0
	1.00	0.0	0.0
Downwards/opposed	0.36	30	10

The flame tip position and the coil position are plotted as a function of time for all samples in *Figure 5*. The warping or displacement of the coils was only significant for the opposed test. Thus, the energy provided by the heating coil was similar in the other tests. The energy provided by the heating coils was 80 J/s or equivalently 80 W. Knowing that the ignition coil covered 13 mm breadth of the 50 mm sample width, the computed heat applied to the edge of the sample was 12.3 W/cm² or 123 kW/m². The convective losses due to the forced flow were identical for each test as the forced flow velocity was the same (20 cm/s). As seen in *Figure 5*, the flame tips exhibited a linear increase over time when the heating coil was energised. Based on the slope of the flame tip position, an increment rate can be extrapolated. The increment rate under concurrent forced flow exhibits a linear dependency as a function of the sample thickness. Such a dependency is expected as the heat loss through the material increases with increasing sample thickness.

For all samples, the flame's leading-edge reached a peak and declined afterwards and eventually extinguishes. Despite the large energy initially received by all the samples in the Saffire II experiments, it is plausible that the deposition of silica-ash was quite substantial, and the flame spread could not continue beyond the initially ignited area without further external energy input. Also, the formation of silica in the solid-phase and the radiative heat losses in the gas-phase (due to microgravity) might have played a role in the failure to achieve flame spread in these tests. A discussion on the transport and deposition of the silica-ash in microgravity is required, though there are no investigations on such a topic. In the following, the behaviour behind the silica-ash transport and deposition will be compared with soot particles.

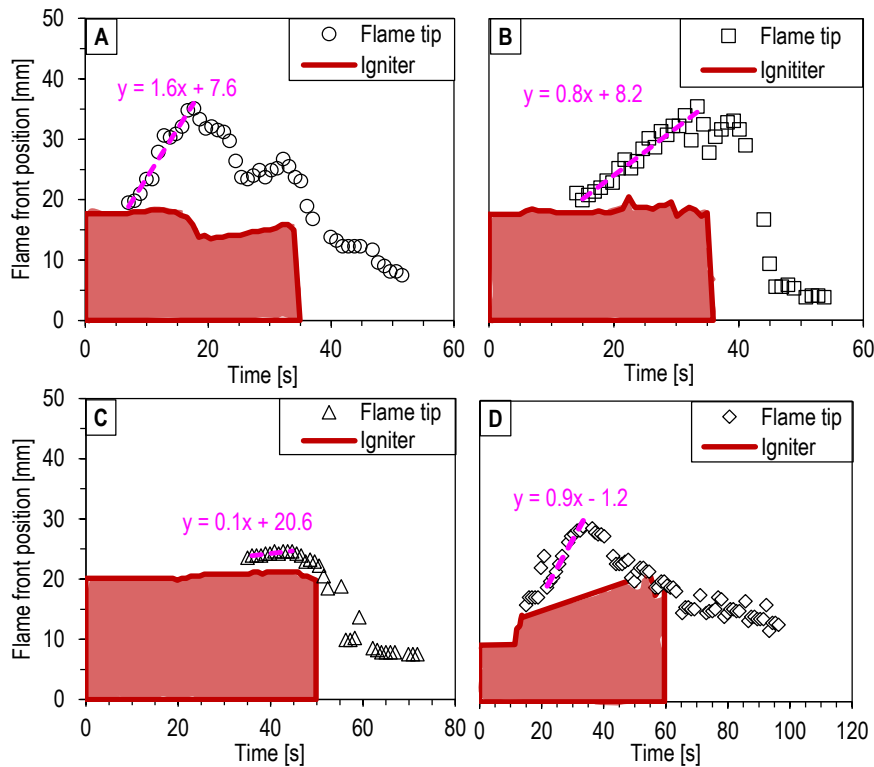


Figure 5 – Flame tip position along with the igniter position for the four PDMS samples tested during the Saffire II tests. A: 0.25 mm (Concurrent), B: 0.61 mm (concurrent), C: 1.02 mm (concurrent), D: 0.36 mm (opposed).

The dominant mechanisms of soot formation in microgravity are defined by residence time and oxidation [36]. In the case of silica-ash, formation occurs during the gas-phase, and there is no information on the leading mechanisms. As neither soot nor silica-ash has a crystalline structure, both can agglomerate to form larger structures. In pyrogenic processes, where silica-ash is formed in a similar fashion as in a diffusion flame on PDMS, the primary silica-ash particles form tightly-bound aggregates that in turn form larger conglomerates [37]. In addition, the primary particle size diameter for soot and silica-ash are in the same order of magnitude, see Table 3. Thus, the thermophoresis process attributed to soot deposition can be used to describe silica-ash transport and deposition in microgravity.

Table 3 – Particulate size length for soot and Silica-ash.

Type	Mean primary particle size diameter [nm]		Problem	Reference
	μg	1 g		
Soot		46	Liquid diffusion flames (toluene, benzene, n-heptane, diethyl ketone)	[38]
	70	30	Flame forming on fluorinated ethylene propylene wire jacket under	[39]
	330	150	Pyrolysis of ethyltetrafluoroethylene wire insulation	[40]
SiO ₂		<100	Amorphous silica ash	[37]

Thermophoresis is a relevant topic within particle deposition, and it refers to the transport of small particles in a temperature gradient (towards the colder region). Thermophoresis forces have been demonstrated to dominate soot deposition on cold walls from gaseous diffusion flames [36,41,42]. Thus, considering thermophoresis is essential to estimate the behaviour of soot deposition on the walls. The velocity induced by thermophoresis, or thermophoretic drift velocity, can be estimated based on the particle size and the temperature gradient. The

thermophoretic deposition is characterised by the thermophoretic velocity. For particles less than 10,000 nm in diameter, the Waldman expression [36] to estimate the thermophoretic velocity is

$$U_t = \frac{3v}{1+(π/8)α_m} \frac{∇T}{T} \quad \text{Equation 2}$$

The estimated and measured thermophoretic velocity for soot particles in microgravity conditions has been reported to be of the order of 0.1 to 1 cm/s [36,38,42].

A reduction in gravity has been shown to result in the increased mean size of soot particles two-fold compared to normal gravity [39,40]. Likewise, the agglomerate sizes have been reported to increase three-fold, which is attributed to thermophoretic forces and long residence times in microgravity [39,43]. The thermophoretic velocity increases with smaller soot particles sizes [38]. For soot deposition, estimated thermophoretic velocities in microgravity were reported to be more than three times larger than estimates based on normal-gravity semi-empirical relation [44].

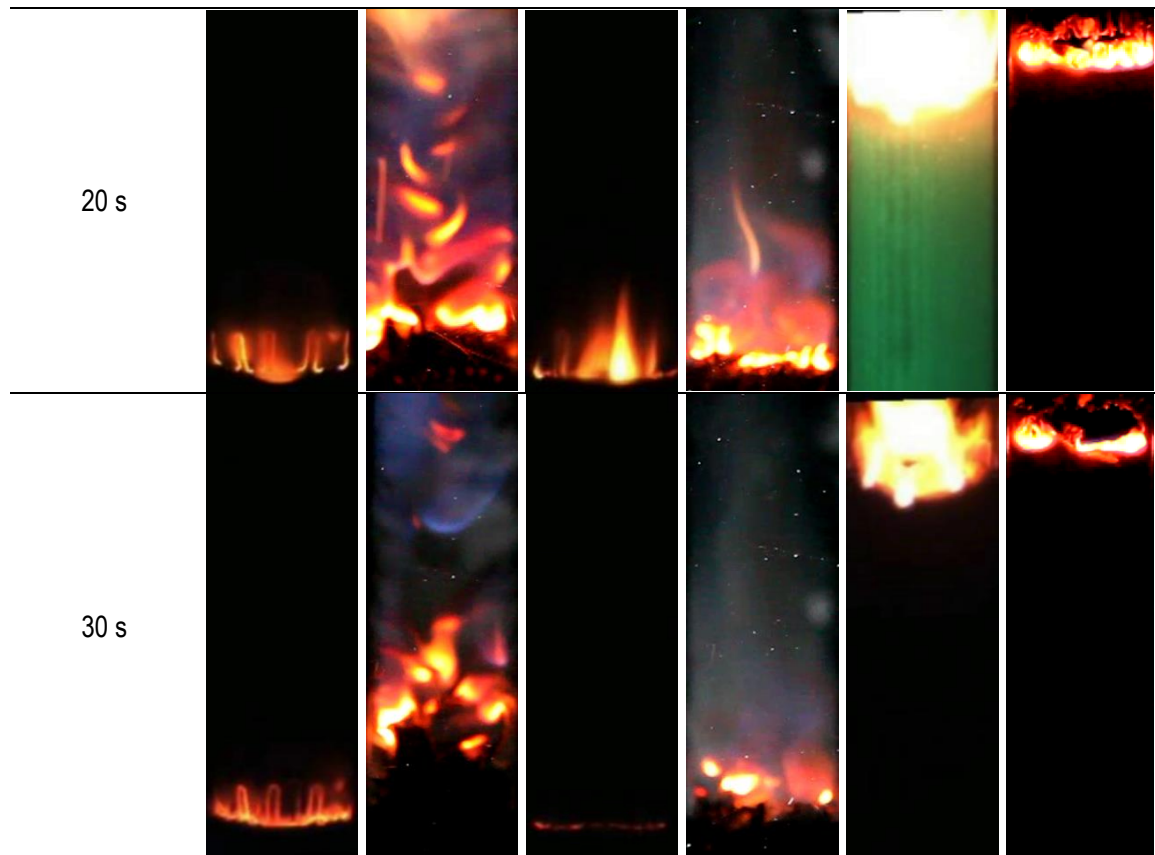
There is a proportional dependency of the thermophoretic velocity of soot particles on the temperature gradient in microgravity [38]. In open-structure aggregates, the thermophoretic forces are dependent on the primary particle size. However, if the morphology of the aggregates is different (closely bound), then these behave as large particles [38]. Silica-ash agglomerates produced in pyrogenic processes can achieve sizes up to 600 nm and have open-fractal morphology [45]. Since silica-ash aggregates might behave akin to soot aggregates in microgravity, the thermophoretic forces can be a dominant factor in the deposition of soot in normal gravity and microgravity scenarios. Thus, soot behaviour will be used to discuss the behaviour of silica-ash in the following sub-chapters.

3.2. Flame spread behaviour in normal gravity

Snapshots taken from the videos of the experiments in normal gravity and microgravity are compared in *Table 4*. Ignition is attained as diffusion flames emerge from both sets of experiments. In the microgravity case, flames were only visible when the heating coil was energised. Once ignitors were off, the flame in microgravity was not self-sustained. On the contrary, in the normal gravity experiments, flames could be established and travelled beyond the region of the igniter.

Table 4 – Comparison of flame spread occurring on PDMS samples of various thicknesses in similar scenarios in microgravity and normal gravity environments. The first snapshot was taken when ignition occurred, the other snapshots were taken in 10-second intervals thereafter. Note: the length of the sample was cut to accommodate all samples in the table, so the width of the samples is 5 cm.

Flow direction		CONCURRENT				OPPOSED	
Sample thickness		0.25mm		0.36mm		0.36mm	
Gravity		μG	1G	μG	1G	μG	1G
Time frame		(t _{ig} = 4 s)	(t _{ig} = 24 s)	(t _{ig} = 18 s)	(t _{ig} = 20 s)	(t _{ig} = 14 s)	(t _{ig} = 42 s)
Ignition							
10 s							



The results obtained in the flow tunnel for flame spread under opposed and concurrent forced flows are presented in the following. In addition, quantification of the silica-ash deposition is also presented in each sub-chapter.

3.2.1. Opposed flow Results

Figure 6 shows a SEM image from a sample taken at the extinction edge from the opposed experiments. The silica-ash thickness appears to be thin compared to the sample thickness. For opposed forced flows, the silica-ash residues measurements are shown in Figure 7. In all cases, the thickness of silica-ash was less than 10 μm , and no dependency is observable at this scale. These results indicate a negligible deposition of silica-ash at the leading edge of an opposed flame in normal gravity scenarios. Gas expansion is the leading mechanism controlling soot motion at the leading edge, and thermophoretic velocities are absent [42]. Thus, only very small quantities of silica-ash deposit on the sample burnout tip.

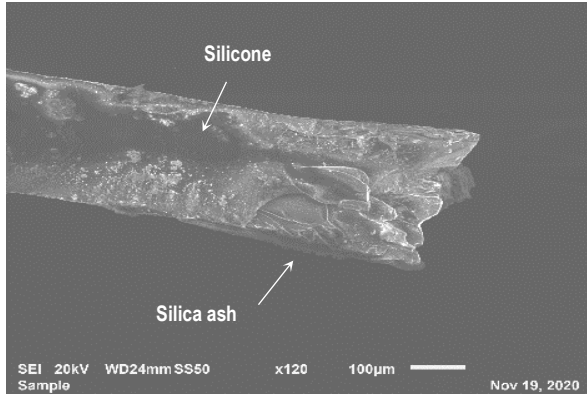


Figure 6 – SEM image of a 0.152 mm sample cross-section from the flow tunnel experiments under opposed forced flows.

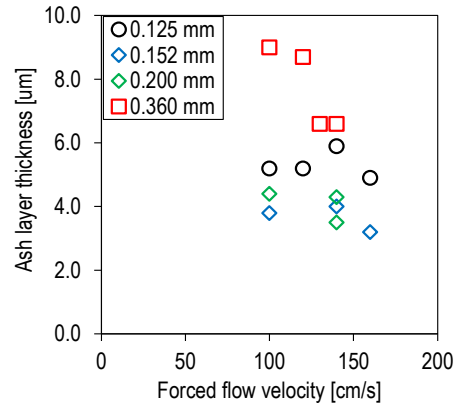


Figure 7 – Silica ash thickness as a function of the opposed, forced flow velocity at the point of extinguishment for various PDMS membranes.

Under buoyant conditions, a characteristic relative velocity is generated for a diffusion flame, and it depends on the thermal characteristic of the gas-phase (temperature changes). Bhattacharjee et al. [46] proposed an expression to compute the characteristic buoyancy-driven flow as $V_{nb} = [(\alpha_g g (T_g - T_0)) / T_0]^{1/3}$. Thus, the forced flows affecting the flame spread can be corrected by adding the characteristic buoyant flow. In the following, the data will be presented as a function of the corrected forced flow ($V_{nb} + V_g$).

The flame spread rates as a function of the opposed forced flows for various PDMS samples is plotted in Figure 8. The flame spread rate decreases with increasing sample thickness, as expected according to the de Ris expression for the flame spread [30]. The flame spread rates exhibit a very small linear dependency for all the samples thicknesses as the forced flow increases. Such behaviour is not consistent with other observations for thermally-thin fuels [23]. In the work of Fernandez-Pello et al. [23], the flame spread rate over a cellulosic fuel decreased slightly with increasing forced flow at 21% oxygen concentration. On the contrary, they reported the opposite for thermally-thick fuels for high oxygen concentrations (>30%). For a thermally-thick material, increasing the forced flow increases the flame attachment, and in turn, the solid-phase receives a larger heat flux from the flame. However, in the case of the thermally-thin PDMS, in-depth losses (or solid-heat up) should be negligible. The results plotted in Figure 8 were obtained in the flow tunnel, where the forced flow started to transition to a turbulent flow at 70-80 cm/s. It is known that for flame radiation is dominant and can become prominent under turbulent flows.

Figure 8 also shows the extinction limit for high forced flow velocities. For extinction conditions where the kinetic effects are important, Fernandez-Pello [47] proposed that $V_{f,o} = V_g^2 / \tau_{chem}$. The expression is very similar to the Damköhler number, which is the ratio of the flow time to the chemical time. If the thermal diffusivity is considered unity, then $V_f \propto Da$. For the conditions of the experiments, the chemistry is not changed since the oxygen concentration remains the same, but the flow time is inversely proportional to the forced flow ($\tau_{flow} = \alpha_g / V_f^2$). Thus, for large forced flow velocities, the Da is reduced via the flow time, and extinction will occur for the opposed flames established over the PDMS samples.

The extinction limit decreases with flow and sample thickness, as seen in Figure 8. Such behaviour cannot be explained by the Damköhler number alone as it only reflects gas-phase chemistry. Intuitively, increasing the sample thickness increases the amount of heat required to decompose the fuel. T'ien, Endo and co-workers [48,49] evaluated the quenching limit of thermally-thick fuels by evaluating the ratio of solid-heat conduction to the heat conduction through the gas-phase, $\Phi = [\lambda_s (\partial T_s / \partial n)_s] / [\lambda_g (\partial T_g / \partial n)_s]$. In that expression, the heating via the temperature gradient is with respect to the normal of the sample surface (∂n) since the sample was spherical. They demonstrated that near-limit phenomena (quenching) are also

dependent on the in-depth heating. For the PDMS, the particularity in its behaviour during flame spread is the formation of silica in the solid-phase. As the sample increases in thickness, the formation of solid-phase silica might increase, and it will affect the heat transfer through the solid-phase. Such a hypothesis most likely explains the behaviour seen in *Figure 8*.

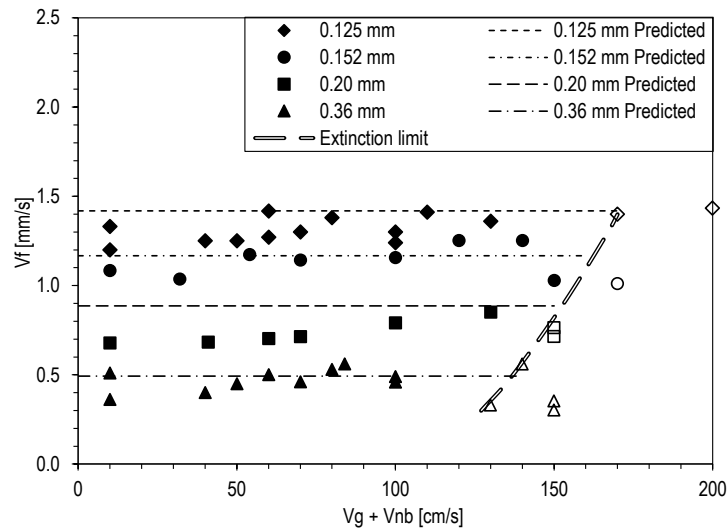


Figure 8 – Measured and predicted opposed flame spread rates for various PDMS thicknesses as a function of the mixed opposed forced flows (buoyant and forced). The data corresponds to the normal (flow tunnel rig). The closed symbols represent propagation conditions, and the filled symbols represent extinction conditions. The extinction limit defines the propagation zone (left) and the extinction zone (right).

It is noticeable that kinetic extinction conditions for PDMS samples occur at high forced flows. By comparison, for a 0.125 mm PMMA film, kinetics become noticeable at 60 cm/s (or roughly 70 cm/s for mixed flow). The gas-phase activation energy for PMMA is most likely higher for the PDMS. This implies that a diffusion flame established over PDMS or other siloxane products are much harder to blow-off.

In *Figure 8*, the theoretical predictions are also plotted. The equation $V_{f,o} = \frac{\lambda}{\rho_s c_p \tau} \left(\frac{T_f - T_v}{T_v - T_\infty} \right)$ was used and is based on the an extended simplified theory (EST) developed by Bhattacharjee, Takahashi and co-workers [28,32,50]. The flame temperature (1200 °C) and the pyrolysis temperature (444 °C) were taken from the literature [3,7]. These do not foresee extinction conditions and were plotted to cover the thermal regime only (before kinetic extinction). The predictions slightly overestimate the experimental normal-gravity results, but they can still be deemed acceptable. Heat conduction from the gas-phase to the solid-phase is dominant for this opposed flame spread over the PDMS samples. Radiation from the gas-phase and surface re-radiation seemed not to be relevant.

3.2.1. Concurrent flow results

An SEM image of the post-burn samples collected after extinction occurred in the concurrent flame spread experiments are depicted in *Figure 9*. The picture shows a very thick SiO₂ layer in the order of half-thickness of the PDMS sample. The SEM image only shows silica ash on one side, as the other side was removed due to mechanical manipulation during SEM measurements. The silica-ash deposition is very significant and more detrimental for the concurrent flame spread case than the opposed case (as seen in the previous sub-chapter). There appear to be no studies on the transport and deposition of silica-ash emerging for diffusion flame spread in normal gravity. Most studies looking at the fire behaviour of silicones and polysiloxanes focus on the overall behaviour or the effect of silica ash on burning parameters [3,19–22]. Lipowitz [3] claimed that silica-ash was deposited on the silicone pool due to the cooling down of the particles emerging from the plume (buoyancy).

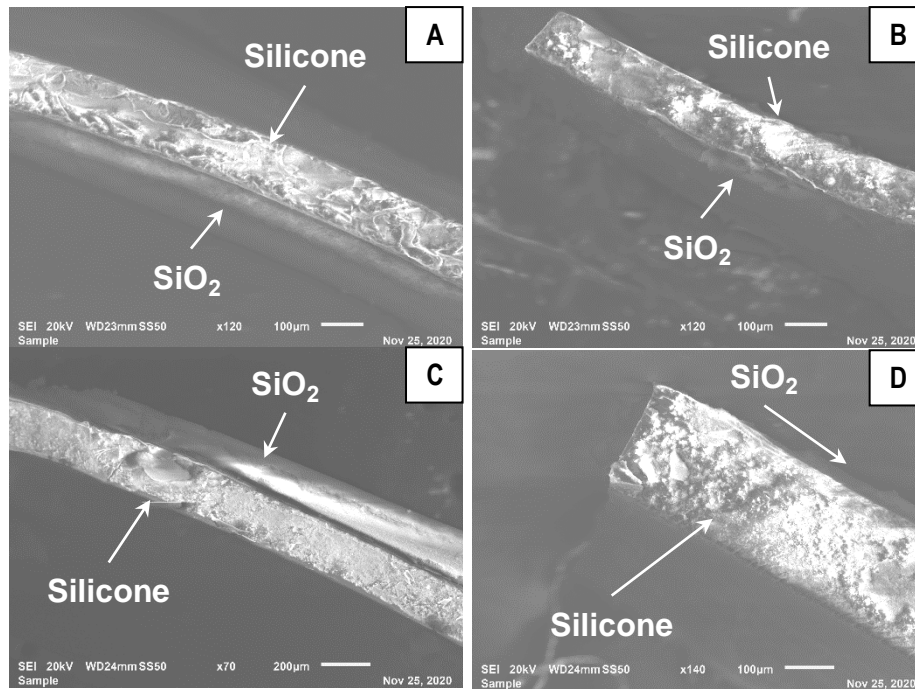


Figure 9 – SEM images of the cross-section of various samples from the flow tunnel experiments under concurrent forced flow. Image A: 0.125 mm PDMS sample under 10 cm/s forced flow at 20 mm distance from the point of extinguishment (X_{ext}). B: 0.125 mm PDMS sample under 10 cm/s forced flow at 40 mm distance from the point of extinguishment (X_{ext}). C: 0.25 mm PDMS sample under 65 cm/s forced flow at 00 mm distance from the point of extinguishment (X_{ext}). D: 0.25 mm PDMS sample under 65 cm/s forced flow at 40 mm distance from the point of extinguishment (X_{ext}).

The profiles of silica-ash thickness for a 0.36 mm PDMS sample are plotted in Figure 10. In the left panel, the silica-ash thickness is at a maximum at the point of extinguishment, and downstream from that point, the thickness decreases in an exponential manner. The deposition process is transient in nature, but as the flame travels upwards, the largest accumulation of ash will occur where the temperature gradient and the flame temperature is highest. According to Equation 2, the thermophoretic velocities are greatest, where the temperature gradient is largest.

By imposing concurrent forced flow, the ash profiles diminish in thickness. The left panel of Figure 10 shows that all the ash thickness profiles have a similar negative exponential behaviour. In fact, all have a similar exponent in their fitting function. The right panel in Figure 10 shows the ash thickness as a function of the forced flow. It can be seen the direct effect of imposing a convective force on the concurrent flame spread. The convective force produces a larger momentum compared to the momentum created by the thermophoretic forces. Thus, part of the silica-ash is transported away without depositing on the downstream unburnt fuel.

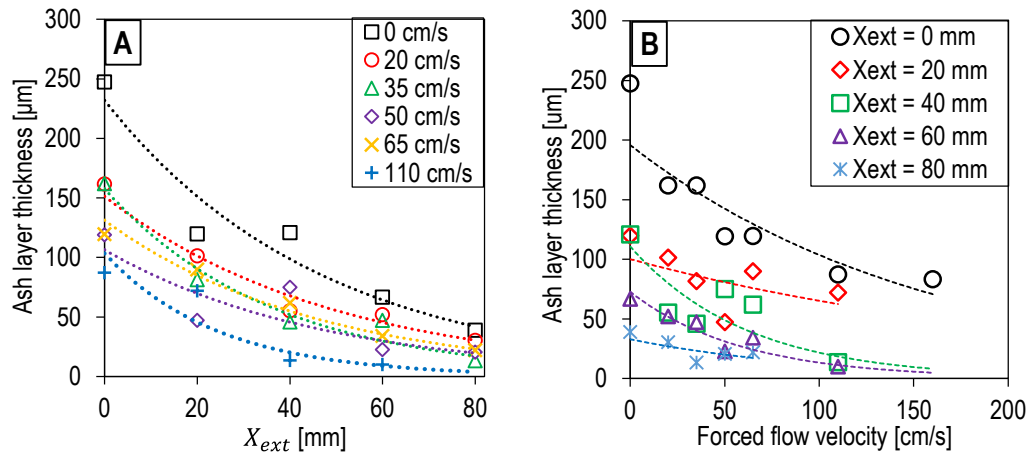


Figure 10 – Silica ash thickness as a function of the concurrent forced flow velocity at various distances from the point of extinguishment for a 0.36 mm thick PDMS sample, as measured using SEM. In the left panel (A), the silica-ash thickness is plotted for various distances downwards from the point of extinguishment (X_{ext}) as a function of the forced flow. The right panel (B) depicts the silica-ash thickness as a function of the forced flow velocity for various distances from the point of extinguishment (X_{ext}).

The normalised silica-ash thickness is plotted as a function of the forced flow for various PDMS sample thicknesses in Figure 11. The ash thickness normalisation was done against the half-thickness of the corresponding PDMS sample. Thus, a dimensionless thickness of unity means that the measured silica-ash was half the thickness of the corresponding sample. There are some discrepancies in the data points in Figure 11, as some silica-ash thicknesses increase with increasing forced flow velocity. During the flame spread experiments, the PDMS sample deformed and warped quite noticeably. Regardless of those points, the profiles in Figure 11 indicate that the convective forces affect the silica-ash deposition.

With increasing sample thickness, the results in Figure 11 do not show a significant increase in silica formation and eventually more deposition (increase in thickness). That is, the silica-ash thickness accumulated is proportionally smaller as the sample thickness increases. Although the precise mechanisms in the formation of silica-ash are not known, unlike soot formation, stoichiometric considerations could be used to explain such behaviour. If the oxidiser concentration remains the same, in this case, air, the number of moles of SiO_2 per mole of fuels remains invariable with respect to the stoichiometric ratio [3]. Only if the local supply of oxidiser is restricted to the combustion zone will the production of silica-ash be affected. It seems that with increasing thickness, there is not enough oxidiser to match the vaporised mass at the combustion zone.

The problem can then be considered fuel-rich, and the oxidiser level would have to increase significantly near the combustion zone to yield more silica-ash.

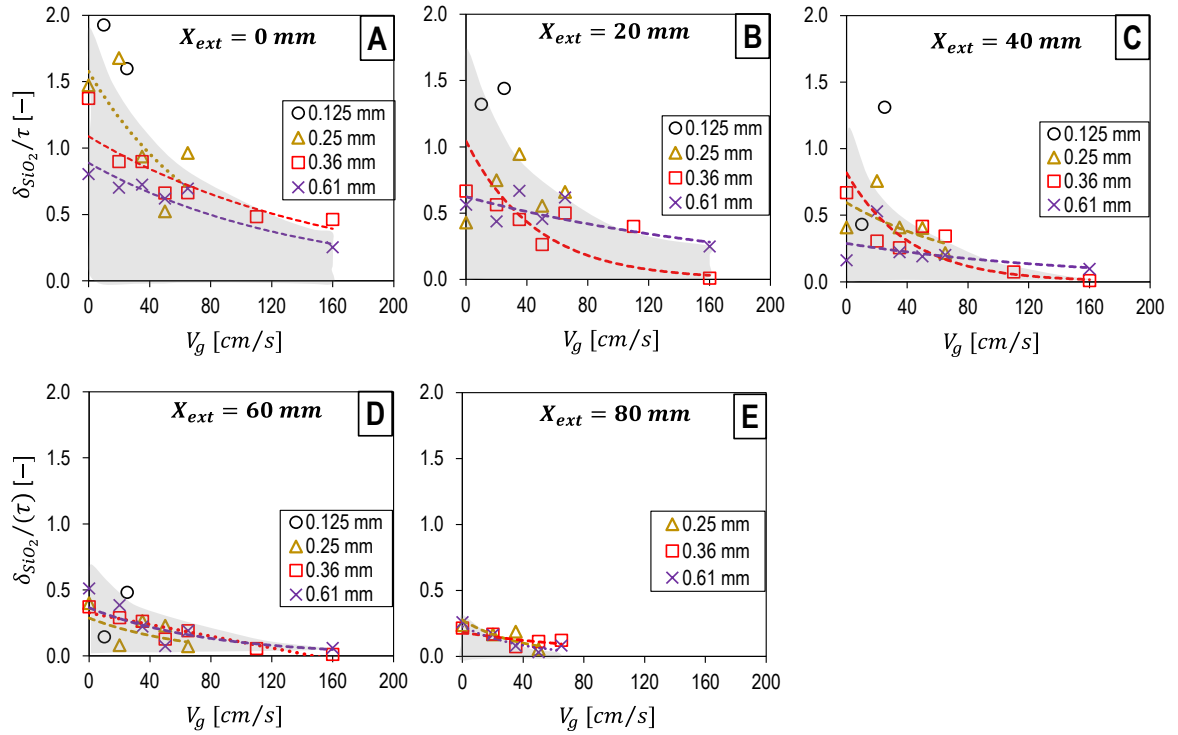


Figure 11 - Normalised silica-ash deposition as a function of the forced concurrent flows at various distances from the point extinguishment (X_{ext}) for various PDMS thicknesses. Panel (A) represents the data measured at the extinction point ($X_{ext} = 0$ mm). Panel (B) represents the data at 20 mm from the point of extinguishment ($X_{ext} = 20$ mm). Panel (C) represents the data at 40 mm from the point of extinguishment ($X_{ext} = 40$ mm). Panel (D) represents the data at 60 mm from the point of extinguishment ($X_{ext} = 60$ mm). Finally, Panel (E) represents the data at 60 mm from the point of extinguishment ($X_{ext} = 60$ mm).

The flame spread rates as a function of the concurrent forced flows for various PDMS samples are plotted in Figure 12. The results for this mode of flame spread are in principle more complex than the previously discussed opposed flame spread cases. The transport and deposition of silica-ash on the sample ahead of the combustion zone is determinant to the heat and mass transfer processes. The transport and deposition of the SiO_2 ash is dominated by two forces – thermophoresis and convection. It was seen that for increasing forced flows, convective forces dominate. Thus, the silica-ash deposition decreases with increasing forced flows. A modified expression for the concurrent flame spread over a thermally-thin material developed by Fernandez-Pello [23] will be used to establish discussions. The modified expression is the following:

$$V_f = l_h \left[\frac{[(\rho_{\text{SiO}_2} c_{\text{SiO}_2} \tau_{\text{SiO}_2}) + (\rho_s c_s \tau)](T_p - T_o)}{(c_1 \lambda_g \rho_p V_g / x)^{1/2} (T_f - T_p) + \dot{q}_{fr}'' + \dot{q}_e'' - \dot{q}_{rs}''} - \frac{c_2 x}{V_g} t_{chem} \right]^{-1} \quad \text{Equation 3}$$

Notice that the effect of silica-ash is incorporated in the heat transfer rate needed to raise the sample temperature to its pyrolysis temperature. Thus, the silica-ash affects the transfer of heat from the flame via convection $(c_1 k_g \rho_p V_g / x)^{1/2}$, flame radiation \dot{q}_{fr}'' or any externally applied heat \dot{q}_e'' . Moreover, surface re-radiation \dot{q}_{rs}'' is also affected by any deposited silica-ash. Another effect of the ash is its deterrent mechanism on pyrolysates and oxidisers' diffusion at the fuel surface. This reduced diffusivity effect can be accounted via the chemical part in the above equation. In Fernandez-Pello's definition of the Damköhler

number ($Da = \frac{A_g \Delta H_R \rho_g E_g Y_{o,\infty} Y_{Fs}}{c_p R T_f^2 Y_g / x} e^{-E/RT_f}$), the reduction of diffusivity reduces the local mass fraction of species, Y_{Fs} , and the mass fraction of oxidiser, $Y_{o,\infty}$.

As seen in *Figure 12*, the flame spread rate at low laminar forced flows is considered a "near-limit" condition as the flame did propagate over the entire sample length. Despite that, the flame spread rate for most of the samples exhibits a linear dependency as a function of the laminar forced flow. Previously, it was shown that silica-ash deposition was nearly exponential concerning distance and laminar forced flows. As the forced flow is increased further, the near-limit behaviour due to excessive silica ash deposition is left behind, and flame spread is practically propagating steadily over the entire sample. For these high forced flows, the deposition of silica ash on the fuel is reduced drastically. As such, the deposition is becoming insignificant, and the flame spread is dominated entirely by the heat and mass transfer along the characteristic flame length. It is worth mentioning observations of the behaviour exhibited by the thinnest sample (0.125 mm). Under propagation conditions, the 0.125 mm thick samples showed a non-monotonic behaviour as the forced flow increased. This behaviour might be associated with the radiative nature of turbulence in the flow. The extinction limit in *Figure 12* is thus dominated by the transport and deposition silica-ash and the sample thickness.

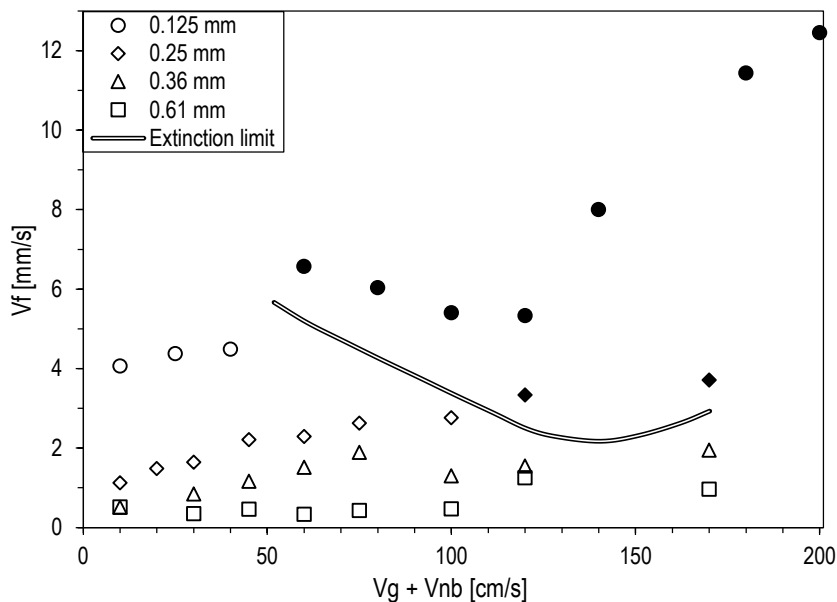


Figure 12 – Flame spread rates for various PDMS samples as a function of the mixed concurrent forced flows (buoyant and forced). The data plotted corresponds to normal-gravity (flow tunnel rig). The open and closed symbols represent extinction and propagation conditions. The extinction region lies below the extinction boundary and above the curve lies the propagation region.

3.3. Flammability map

The flammability map with data points from normal gravity and microgravity experiments is shown in *Figure 13*. The boundaries are plotted as a function of the forced flow and sample thickness. As seen, the contrasting near-limit behaviour for the flame spread between opposed and concurrent flame spread is due to various dominant forces. The opposed flame spread extinction map shows that flames are predominantly viable for extensive forced flows. Extinction occurs via kinetics for a specific sample under increasing forced flows (moving leftwards in the map). However, for increasing sample thickness (moving upwards in the map), extinction occurs due to insufficient energy to counteract the energy loss to break through the material. The dominant mechanisms for near-limit under concurrent forced flows are directly dependent on the transport and deposition of silica-ash and the sample thickness (via thermal penetration).

The microgravity data points from Saffire II are also plotted in *Figure 13*. For the concurrent case, the microgravity data lies within the extinction flammability region obtained in normal-gravity scenarios. This

suggests that concurrent flame spread over a PDMS sample is primarily dominated by silica-ash transport and deposition in microgravity as well. However, the single data point obtained in microgravity disagrees with the normal-gravity flammable region when comparing the opposed case. This behaviour might also suggest that silica-ash transport dominates opposed flame spread in microgravity, but it is not clear to which extent. From *Figure 13*, it is clear that the most critical scenario would be for flame travelling under opposed forced flows over a very thermally-thin sample. If this flammability map were available before designing Saffire II tests, it would have been obvious which PDMS thicknesses and conditions would have been most appropriate for the flight experiments.

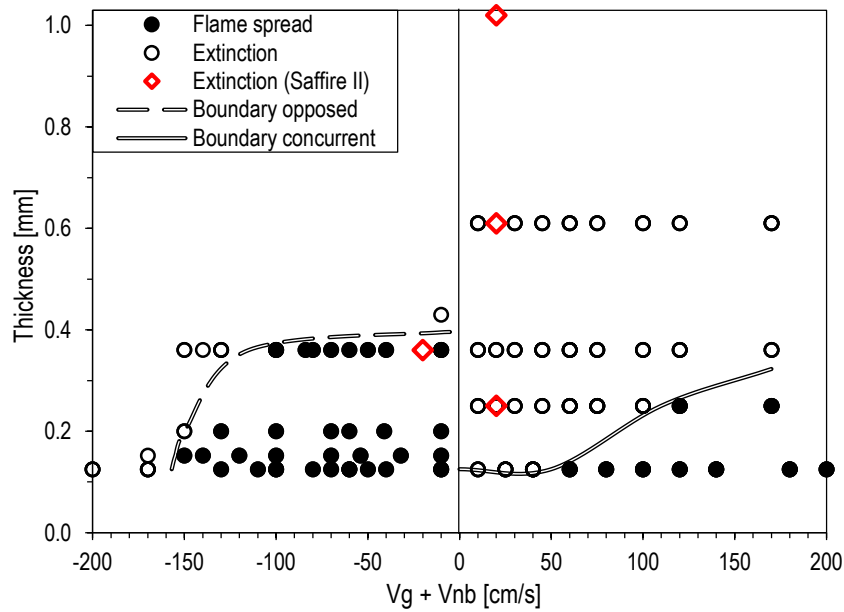


Figure 13 – Extinction boundary limits for PDMS membranes for a range of mixed flow velocities and sample thicknesses. The negative and positive axes represent opposed and concurrent forced flows, respectively. The data corresponds to normal (flow tunnel rig) and microgravity (Saffire II). The closed and open symbols represent propagation and extinction conditions, respectively.

4. Conclusion

Experimental work was carried to investigate the flame spread behaviour on polydimethylsiloxanes (PDMS) membranes under concurrent and opposed forced flows. The experiments were predominantly conducted in normal gravity but can provide relevant information on the PDMS membranes in microgravity conditions through comparison with spacecraft experiments.

Under concurrent forced flows, the flame spread was heavily dominated by the transport and deposition of silica-ash, which greatly affected the heat balance. The concurrent flame spread was only viable when the forced flow was sufficiently high to depress the silica-ash deposition (convective momentum much larger than thermophoretic forces). Consequently, the concurrent flame rates were very unstable at low forced flows but stable at high forced flows, with estimates ranging from 0.1 to 12 mm/s. For opposed flame spread, the silica-ash deposition can be deemed negligible under normal-gravity conditions. Opposed flame spread rates were stable, with values ranging from 0.5 to 1.5 mm/s.

The effect of the forced flow intensity on silica-ash deposition was dominated by concurrent flames' near-limit behaviour. By contrast, the extinction behaviour of opposed flame spread was dominated by two phenomena. For high velocity forced flows, kinetics was the dominant mechanism for extinction, while for increasing thickness, the formation of silica via the solid-phase dominated the extinction of opposed flame spread. Therefore, the microgravity results from the Saffire II experiments can also be explained by the silica-ash deposition and transport, as these effects become even more relevant in the absence of gravity through the altered heat and mass transfer in such conditions.

From the flammability map created in the current study, it is clear that the most critical scenario for PDMS membranes occurs under opposed forced flows and if they are thermally-thin. Thus, PDMS membranes might offer an improved flammability behaviour in microgravity for a range of scenarios where the sample is not falling under the category of thermally-thin behaviour.

Under the experimental conditions seen, the Saffire II test might indicate that the PDMS might be less flammable in microgravity than in normal gravity due to the transport and deposition of silica-ash. If such a postulate were accurate, then PDMS and other silicone-based materials could be considered safer for spacecraft applications. Materials for spacecraft applications could be improved (reducing their flammability) using silicone composites or silicone coating as a passive strategy. Thus, more work is required to fully understand the formation of silica-ash and its transport and deposition in normal and microgravity environments.

Acknowledgements

The authors are grateful for the insights and support provided by the SAFFIRE project. Finally, the authors are particularly grateful to the School of Engineering at the University of Edinburgh for funding the main author's PhD programme.

References

- [1] I. Hong, S. Lee, Cure kinetics and modeling the reaction of silicone rubber, *J. Ind. Eng. Chem.* 19 (2012) 42–47. doi:10.1016/j.jiec.2012.05.006.
- [2] A.C.M. Kuo, Poly(dimethylsiloxane), in: *Polym. Data Handb.*, Oxford University Press, 1999: pp. 411–435. doi:10.1007/978-1-4419-6247-8_9030.
- [3] J. Lipowitz, Flammability of poly(dimethylsiloxanes). I. A model for combustion, *Fire Flammabl.* 7 (1976) 482–503.
- [4] S. Hamdani, C. Longuet, D. Perrin, J.M. Lopez-cuesta, F. Ganachaud, Flame retardancy of silicone-based materials, *Polym. Degrad. Stab.* 94 (2009) 465–495. doi:10.1016/j.polymdegradstab.2008.11.019.
- [5] G. Camino, S.M. Lomakin, M. Lazzari, Polydimethylsiloxane thermal degradation. Part 1. Kinetic aspects., *Polymer (Guildf).* 42 (2001) 2395–2402.
- [6] NASA, Flammability, offgassing, and compatibility requirements and test procedures. NASA-STD-6001B, (2016) 1–158.
- [7] J.E. Niehaus, P. V Ferkul, S.A. Gokoglu, G.A. Ruff, Buoyant Effects on the Flammability of Silicone Samples Planned for the Spacecraft Fire Experiment (Saffire), in: *45th Int. Conf. Environ. Syst.* 12-16, Bellevue, Washington, 2015.
- [8] *Recapturing a Future for Space Exploration: Life and Physical Sciences Research for a New Era*, The National Academies Press, Washington, D.C, 2012.
- [9] G. Jomaas, J.L. Torero, C. Eigenbrod, S.L. Olson, P. V. Ferkul, G. Legros, A.C. Fernandez-Pello, A.J. Cowlard, S. Rouvreau, N. Smirnov, O. Fujita, J.S. T'ien, G.A. Ruff, D.L. Urban, Fire Safety in Space – Beyond Flammability Testing of Small Samples, *Acta Astronaut.* 109 (2015) 208–216.
- [10] D.L. Urban, P. Ferkul, S. Olson, G.A. Ruff, S.T. James, Y.T. Liao, A.C. Fernandez-Pello, J.L. Torero, G. Legros, C. Eigenbrod, N. Smirnov, O. Fujita, S. Rouvreau, B. Toth, G. Jomaas, Flame Spread: Effects of Microgravity and Scale, *Combust. Flame.* 199 (2018) 1–22. doi:10.1016/j.combustflame.2018.10.012.
- [11] S.K. Srivastava, T. Kuila, Fire Retardancy of Elastomers and Elastomer Nanocomposites, Elsevier B.V., 2014. doi:10.1016/B978-0-444-53808-6.00018-4.
- [12] A.S. Kuz'minskii, Y.A. Goldovskii, Investigation of the oxidation of polydimethylsiloxane rubbers, *Polym. Sci. U.S.S.R.* 3 (1962) 823–832. doi:10.1016/0032-3950(62)90158-2.
- [13] T.H. Thomas, T.C. Kendrick, Thermal analysis of polydimethylsiloxanes. I. Thermal degradation in controlled atmospheres, *J. Polym. Sci. Part A-2 Polym. Phys.* 7 (1969) 537–549. doi:10.1002/pol.1969.160070308.
- [14] N. Grassie, K.F. Francey, I.G. MacFarlane, The thermal degradation of polysiloxanes - Part 4: poly(dimethyl/diphenyl siloxane), *Polym. Degrad. Stab.* 2 (1980) 67–83.
- [15] N. Grassie, I.G. MacFarlane, The Thermal Degradation of Polysiloxanes - I, *Eur. Polym. J.* 14 (1978) 875–884.
- [16] M. Zeldin, D.W. Kang, G.P. Rajendran, B. Qian, S.J. Choi, Kinetics of thermal depolymerisation of trimethylsiloxy end-blocked polydimethylsiloxane and polydimethylsiloxane-n-phenylsilazane copolymer, *Sci. Total Environ.* 73 (1988) 71–85.
- [17] T.S. Radhakrishnan, New method for evaluation of kinetic parameters and mechanism of degradation from pyrolysis-GC studies: thermal degradation of PDMS, *J. Appl. Polym. Sci.* 73 (1999) 441–450.

- [18] G. Camino, S.M. Lomakin, M. Lageard, Thermal polydimethylsiloxane degradation. Part 2. The degradation mechanisms, *Polymer (Guildf)*. 43 (2002) 2011–2015. doi:10.1016/S0032-3861(01)00785-6.
- [19] R.R. Buch, Rates of heat release and related fire parameters for silicones, *Fire Saf. J.* 17 (1991) 1–12. doi:0379-7112/91.
- [20] R. Buch, J. Shields, T. Kashiwagi, T. Cleary, K. Steckler, The Influence of Surface Silica on the Pyrolysis of Silicones, in: K.A. Beall (Ed.), *Annu. Conf. Fire Res.*, NIST, 1998.
- [21] F.-Y. Hshieh, Shielding effects of silica-ash layer on the combustion of silicones and their possible applications on the fire retardancy of organic polymers, *Fire Mater.* 22 (1998) 69–76.
- [22] F.Y. Hshieh, R.R. Buch, Controlled-atmosphere cone calorimeter studies of silicones, *Fire Mater.* 21 (1997) 265–270. doi:10.1002/(SICI)1099-1018(199711/12)21:6<265::AID-FAM620>3.0.CO;2-U.
- [23] A.C. Fernandez-pello, The Solid Phase, in: *Combust. Fundam. Fire*, 1995: pp. 10–18.
- [24] J.L. Torero, Heat and mass transfer in fires: Scaling laws and their application, in: *12th Int. Meet. Heat Transf.*, Tangiers, Morocco, 2005.
- [25] S. Takahashi, M. Kondou, K. Wakai, S. Bhattacharjee, Effect of radiation loss on flame spread over a thin PMMA sheet in microgravity, *Proc. Combust. Inst.* 29 (2002) 2579–2586. doi:10.1016/S1540-7489(02)80314-5.
- [26] S. Bhattacharjee, K. Wakai, S. Takahashi, Flame spread in a microgravity environment - Role of fuel thickness, in: *Sixth Int. Microgravity Combust. Work.*, National Aeronautics and Space Administration NASA, Cleveland, Ohio, 2001: pp. 405–408.
- [27] S. Bhattacharjee, C. Paolini, K. Wakai, S. Takahashi, Extinction criteria for opposed-flow flame spread in a microgravity environment, in: *Seventh Int. Work. Microgravity Combust. Chem. React. Syst.*, National Aeronautics and Space Administration NASA, Cleveland, Ohio, 2003: pp. 201–204.
- [28] S. Bhattacharjee, R. Ayala, K. Wakai, S. Takahashi, Opposed-flow flame spread in microgravity-theoretical prediction of spread rate and flammability map, *Proc. Combust. Inst.* 30 (2005) 2279–2286. doi:10.1016/j.proci.2004.08.020.
- [29] P. Ferkul, S. Olson, D.L. Urban, G.A. Ruff, J. Easton, J.S. T'ien, Y.-T.T. Liao, A.C. Fernandez-Pello, J.L. Torero, C. Eigenbrod, G. Legros, N. Smirnov, F. Osamu, S. Rouvreau, B. Toth, G. Jomaas, Results of Large-Scale Spacecraft Flammability Tests, in: *47th Int. Conf. Environ. Syst. ICES*, 2017.
- [30] J.N. De Ris, Spread of a laminar diffusion flame, *Symp. Combust.* 12 (1969) 241–252. doi:10.1016/S0082-0784(69)80407-8.
- [31] S. Takahashi, Y. Seki, T. Ihara, K. Wakai, S. Bhattacharjee, Effect of Sample Width on Flame Spread Rate over a Thin Material in Microgravity, *Trans. Japan Soc. Aeronaut. Sp. Sci. Sp. Technol. Japan.* 7 (2009) 61–66. doi:10.2322/tstj.7.Ph_61.
- [32] S. Takahashi, M. Hotta, S. Bhattacharjee, T. Ihara, K. Wakai, Classification of Flame Spread Behavior over a Solid Material by Scale Analysis (In Japanese), *日本マイクログラビティ応用学会誌.* 29 (2012) 23–31.
- [33] S. Takahashi, S. Bhattacharjee, T. Ihara, K. WAKAI, Effect of Ambient Gas on Flame Spread over a Solid Material in Microgravity, *JASMA J. Japan Soc. Microgravity Appl. = 日本マイクログラビティ応用学会誌.* 24 (2007) 225–230. <http://ci.nii.ac.jp/naid/10020006647/>.
- [34] S.Y. Hsu, J.S. T'ien, Flame spread over solids in buoyant and forced concurrent flows: Model computations and comparison with experiments, *Proc. Combust. Inst.* 33 (2011) 2433–2440. doi:10.1016/j.proci.2010.05.093.
- [35] O. Fujita, Solid combustion research in microgravity as a basis of fire safety in space, *Proc. Combust. Inst.* 35 (2015) 2487–2502.

- [36] J.H. Choi, O. Fujita, T. Tsuiki, J. Kim, S.H. Chung, In-situ observation of the soot deposition process on a solid wall with a diffusion flame along the wall, *JSME Int. Journal, Ser. B Fluids Therm. Eng.* 49 (2006) 167–175. doi:10.1299/jsmeb.49.167.
- [37] C. Graf, Silica, amorphous, *Kirk-Othmer Encycl. Chem. Technol.* (2018) 1–43.
- [38] H. Ono, R. Dobashi, T. Sakuraya, Thermophoretic velocity measurements of soot particles under a microgravity condition, *Proc. Combust. Inst.* 29 (2002) 2375–2382. doi:10.1016/s1540-7489(02)80289-9.
- [39] J.F. Guan, J. Fang, Y. Xue, J.W. Wang, J. jun Wang, Y.M. Zhang, Morphology and concentration of smoke from fluorinated ethylene propylene wire insulation in microgravity under forced airflow, *J. Hazard. Mater.* 320 (2016) 602–611. doi:10.1016/j.jhazmat.2016.07.056.
- [40] M. Paul, F. Issacci, I. Catton, G.E. Apostolakis, Characterization of smoke particles generated in terrestrial and microgravity environments, *Fire Saf. J.* 28 (1997) 233–252. doi:10.1016/S0379-7112(96)00078-1.
- [41] J.H. Choi, O. Fujita, T. Tsuiki, J. Kim, S.H. Chung, A study of the effect of oxygen concentration on the soot deposition process in a diffusion flame along a solid wall by in-situ observations in microgravity, *JSME Int. Journal, Ser. B Fluids Therm. Eng.* 48 (2006) 839–848. doi:10.1299/jsmeb.48.839.
- [42] J.H. Choi, J. Kim, S.K. Choi, B.H. Jeon, O. Fujita, S.H. Chung, Numerical simulation on soot deposition process in laminar ethylene diffusion flames under a microgravity condition, *J. Mech. Sci. Technol.* 23 (2009) 707–716. doi:10.1007/s12206-009-0203-0.
- [43] O. Fujita, K. Ito, H. Ito, Y. Takeshita, Effect of thermophoretic force on soot agglomeration process in diffusion flames under microgravity, in: *NASA Conf. Publ.*, 1997: pp. 217–222.
- [44] A. Toda, Y. Ohi, R. Dobashi, T. Hirano, T. Sakuraya, Accurate measurement of thermophoretic effect in microgravity, *J. Chem. Phys.* 105 (1996) 7083–7087. doi:10.1063/1.472510.
- [45] R.R. Retamal Marín, F. Babick, G.G. Lindner, M. Wiemann, M. Stintz, Effects of sample preparation on particle size distributions of different types of silica in suspensions, *Nanomaterials.* 8 (2018). doi:10.3390/nano8070454.
- [46] S. Bhattacharjee, M. Laue, L. Carmignani, P. Ferkul, S. Olson, Opposed-flow flame spread: A comparison of microgravity and normal gravity experiments to establish the thermal regime, *Fire Saf. J.* 79 (2016) 111–118. doi:10.1016/j.firesaf.2015.11.011.
- [47] G. Cox, *Combustion fundamentals of fire*, Academic, London, San Diego, 1995.
- [48] M. Endo, J.S. T'ien, P. V. Ferkul, S.L. Olson, M.C. Johnston, Flame Growth Around a Spherical Solid Fuel in Low Speed Forced Flow in Microgravity, *Fire Technol.* 56 (2020) 5–32. doi:10.1007/s10694-019-00848-2.
- [49] C.T. Yang, J.S. T'ien, Numerical simulation of combustion and extinction of a solid cylinder in low-speed cross flow, *J. Heat Transfer.* 120 (1998) 1055–1063. doi:10.1115/1.2825890.
- [50] S. Takahashi, K. Maruta, Prediction of Limiting Oxygen Concentration of Thin Materials in Microgravity, *Trans. Japan Soc. Aeronaut. Sp. Sci. Aerosp. Technol. Japan.* 16 (2018) 28–34. doi:10.2322/tastj.16.28.